Termolecular Rate Coefficients and the Standard Enthalpy of the Reaction $OH + CS_2 + M \rightarrow HOCS_2 + M$

Eric Wei-Guang Diau and Yuan-Pern Lee*,†

Department of Chemistry, National Tsing Hua University, 101, Sec. 2, Kuang Fu Road, Hsinchu, Taiwan 30043, R.O.C. *(Received: May 1, 1990; In Final Form: July 2, 1990)*

The reaction between OH and CS_2 has been studied in He in the pressure range 9–270 Torr and the temperature range 249–298 K by means of the laser-photolysis/laser-induced-fluorescence technique. Analysis of the temporal profile of [OH] yielded the rate coefficients for the forward and reverse reactions for the equilibrium $OH + CS_2 + M \rightleftharpoons HOCS_2 + M$ and hence the equilibrium constant. Study of the temperature dependence of the equilibrium constant leads to the standard enthalpy of reaction $\Delta H^\circ = -43.9 \pm 5.3$ kJ mol^{-1} and the standard entropy of reaction $\Delta S^\circ = -102.9 \pm 15.4$ J K^{-1} mol^{-1}. The termolecular rate coefficients for the forward reaction at 298 K have also been determined to be $k^{III}_{He} = (5.04 \pm 1.01) \times 10^{-32}$ cm^6 molecule^{-2} s^{-1} and $k^{III}_{CS_2} = (4.28 \pm 1.07) \times 10^{-31}$ cm^6 molecule^{-2} s^{-1}. The rate coefficients for the reverse reaction at 298 K have been determined to be $k^{R}_{He} = (7.36 \pm 1.47) \times 10^{-15}$ cm^3 molecule^{-1} s^{-1} and $k^{R}_{CS_2} = (5.79 \pm 1.45) \times 10^{-14}$ cm^3 molecule^{-1} s^{-1}. All uncertainties represent 95% confidence limits. The temperature dependence of k^{III}_{He} and k^{R}_{He} corresponds to activation energies $E_a = -13.4 \pm 3.4$ and 34.6 ± 8.7 kJ mol^{-1}, respectively. For the reaction also studied in Ar at 246 K, consistent results have been obtained.

Introduction

The reaction between OH and CS_2 is important in the chemistry of the atmosphere.[1] The end products of this reaction in air, identified to be OCS and SO_2,[2-4] have a major environmental impact on both climatic change and acid deposition. Laboratory studies of this reaction have produced contradictory results for the rate coefficients. Whereas Kurylo[5,6] and Cox and Sheppard[7] reported rate coefficients of $(1.85–3) \times 10^{-13}$ cm^3 molecule^{-1} s^{-1}, in other investigations based on the flash-photolysis,[8,9] the discharge-flow,[10,11] or the competitive-reaction techniques[12] much smaller values of the rate coefficients, of the order of 10^{-15} cm^3 molecule^{-1} s^{-1}, were obtained. In the presence of O_2, apparent rate coefficients $\simeq 2 \times 10^{-12}$ cm^3 molecule^{-1} s^{-1} for the title reaction have been determined by means of the competitive-reaction technique.[2-4] A reaction mechanism which consists of an equilibrium in the formation of an adduct, followed by the reaction of the adduct with O_2, was proposed to interpret the observed rate enhancement due to O_2:

$$OH + CS_2 \overset{M}{\rightleftharpoons} HOCS_2 \quad (1)$$

$$HOCS_2 + O_2 \rightarrow \text{products} \quad (2)$$

In the early flash-photolysis experiments, there was no evidence of the adduct formation on the millisecond time scale. Recently, Hynes et al. employed the laser-photolysis/laser-induced-fluorescence technique and detected an equilibrium in reaction 1 on the time scale of approximately 10 μs.[13] Analysis of the observed temporal profile of [OH] yielded the forward and the reverse rate coefficients, and hence the equilibrium constant for reaction 1. The standard enthalpy of reaction $\Delta H^\circ = -41.4 \pm 5.0$ kJ mol^{-1} for reaction 1 was obtained from the temperature dependence of the equilibrium constant. Bulatov et al.,[14] applying a similar technique except for a different method for the generation of OH, determined an equilibrium constant about twice that reported by Hynes et al. at 298 K; they did not study the temperature dependence of the equilibrium constant. Recently, Ravishankara and co-workers, employing a similar technique to that of Hynes et al., determined $\Delta H^\circ_{298} = -45.6 \pm 4.2$ kJ mol^{-1} and $\Delta S^\circ_{298} = -100.5 \pm 18.4$ J K^{-1} mol^{-1}.[15] Whereas the reported values of ΔH° differed by only 4.2 kJ mol^{-1}, the equilibrium constants determined by Ravishankara and co-workers are about twice those reported near 250 K by Hynes et al., and about 40% greater at 298 K. In none of these studies was the effect of the CS_2 molecule considered as a third body on the termolecular reaction, although a relatively large concentration of CS_2 was employed. Furthermore, because these three investigations were concerned mainly with the equilibrium constants of reaction 1, the termolecular rate coefficients for reaction 1 were not determined.

We have investigated the title reaction by means of the laser-photolysis/laser-induced-fluorescence technique. Through a careful control of experimental conditions and an improved analysis of the [OH] temporal profile, we have been able to determine accurately not only the equilibrium constant but also the termolecular rate coefficients for M = He and M = CS_2.

Experimental Section

The OH radicals were generated by pulsed-laser photolysis of H_2O_2 and detected by the pulsed laser induced fluorescence technique. The technique and the experimental setup have been described in detail previously;[16] hence only a summary is given here.

The 248-nm output (6–12 mJ/pulse) of a KrF laser was used to photolyze H_2O_2. After a certain delay, the OH radicals were excited by a frequency-doubled dye laser which was pumped by the 532-nm emission of a Nd:YAG laser. The $Q_1(1)$ line of the

† Also affiliated with the Institute of Atomic and Molecular Sciences, Academia Sinica, Taiwan, R.O.C.

(1) Golden, P. D.; Kuster, W. C.; Albritton, D. L.; Fehsenfeld, F. C. *J. Atmos. Chem.* **1987**, *5*, 439 and references therein.
(2) Jones, B. M. R.; Burrows, J. P.; Penkett, S. A. *Chem. Phys. Lett.* **1982**, *88*, 372.
(3) Jones, B. M. R.; Cox, R. A.; Penkett, S. A. *J. Atmos. Chem.* **1983**, *1*, 65.
(4) Barnes, I.; Becker, K. H.; Fink, E. H.; Reimer, A.; Zabel, F.; Niki, H. *Int. J. Chem. Kinet.* **1983**, *15*, 631.
(5) Kurylo, M. J. *Chem. Phys. Lett.* **1978**, *58*, 238.
(6) Kurylo, M. J.; Laufer, A. H. *J. Chem. Phys.* **1979**, *70*, 2032.
(7) Cox, R. A.; Sheppard, D. *Nature* **1980**, *284*, 330.
(8) Atkinson, R.; Perry, R. A.; Pitts, J. N., Jr. *Chem. Phys. Lett.* **1978**, *54*, 14.
(9) Wine, P. H.; Shah, R. C.; Ravishankara, A. R. *J. Phys. Chem.* **1980**, *84*, 2499.
(10) Leu, M. T.; Smith, R. H. *J. Phys. Chem.* **1982**, *86*, 958.
(11) Biermann, H. W.; Harris, G. W.; Pitts, J. N., Jr. *J. Phys. Chem.* **1982**, *86*, 2958.
(12) Iyer, R. S.; Rowland, F. S. *Geophys. Res. Lett.* **1980**, *7*, 797.
(13) Hynes, A. J.; Wine, P. H.; Nicovich, J. M. *J. Phys. Chem.* **1988**, *92*, 3846.
(14) Bulatov, V. P.; Cheskis, S. G.; Iogansen, A. A.; Kulakov, P. V.; Sarkisov, O. M.; Hassinen, E. *Chem. Phys. Lett.* **1988**, *153*, 258.
(15) Murrells, T. P.; Lovejoy, E. R.; Ravishankara, A. R. *J. Phys. Chem.* **1990**, *94*, 2381.
(16) Diau, E. W.-G.; Tso, T.-L.; Lee, Y.-P. *J. Phys. Chem.* **1990**, *94*, 5261.

0022-3654/91/2095-0379$02.50/0

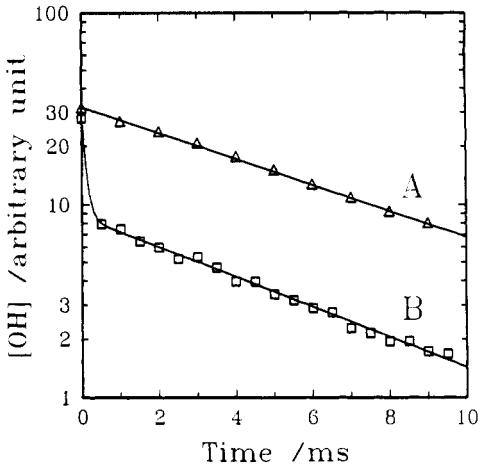

Figure 1. Decay plots of [OH] in the millisecond range. (A) $[CS_2]$ = 0, (B) $[CS_2] = 1.65 \times 10^{16}$ molecules cm^{-3}; $T = 253$ K, $P = 76$ Torr, $[OH]_0 \simeq 3 \times 10^{11}$ molecules cm^{-3}.

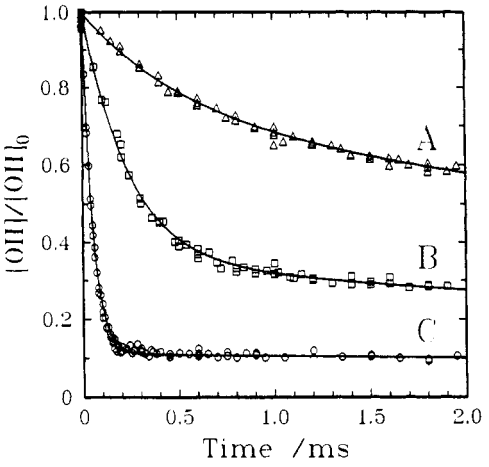

Figure 2. Decay plots of [OH] in the microsecond range. $T = 249$ K, $P = 52$ Torr, $[OH]_0 \simeq 1 \times 10^{11}$ molecules cm^{-3}. $[CS_2]/10^{16}$ molecules cm^{-3} = 0.18 (A); 0.72 (B); 3.36 (C).

$A\ ^2\Sigma^+(v'=1) \leftarrow X\ ^2\Pi(v''=0)$ transition of OH at 282 nm was used for excitation. The fluorescence about 309.6 nm was collected in the direction perpendicular to both the excitation and photolysis axes through a lens and an interference filter (fwhm $\simeq$ 12 nm, 43% transmission at 309.6 nm), and detected by a photomultiplier. The output of the photomultiplier was amplified and averaged with a boxcar integrator.

The concentration of OH is proportional to the integrated intensity of the OH fluorescence. The scattered light (typically relatively small) was subtracted from the observed total emission to give the intensity of the OH fluorescence signal. We measured the intensity of the scattered light in each decay measurement by determining the observed emission with the photolysis laser blocked or with the probe laser fired after a long delay (98 ms) from the photolysis pulse. The temporal profile of the OH concentration was obtained by the measurement of the fluorescence signal with various intervals between the photolysis laser and the probe laser. The repetition rates of both lasers were set at 10 Hz, and the fluorescence signal was averaged over 100 pulses at each delay. Typically, 4–5 sets of data were combined to produce one temporal profile in order to characterize fully both the rapid and the slow components of the profile. Each set of data consisted of 20 points with evenly spaced time delays; the maximum time delay in each set was in the range 0.1–20 ms. The data were normalized to the energy of the excitation laser so as to avoid possible error due to occasional variation of the output energy; the variation was commonly within ±10%. The stability from pulse to pulse was typically within ±3% for the photolysis laser.

A jacketed reaction cell with an internal volume about 150 cm^3 was used in the experiments. It was maintained at constant temperature by circulation of ethanol or water from a thermostated bath through the outer jacket. The temperature of the reactants was measured with a calibrated thermocouple inserted into the reactor. All experiments were carried out under "slow flow" conditions so as to replenish the reactants.

The diluent gas He (99.9995%) was used without further purification. H_2O_2 (~90%) and CS_2 (99.9%) were thoroughly degassed prior to use. A small amount of He bubbled through the solution carried the H_2O_2 into the cell. The flow rate of CS_2 was determined by measurement of the rate of pressure increase in a calibrated volume. To investigate whether part of the CS_2 was adsorbed on the wall of the reactor, the photoabsorption at 214 nm ($\sigma = 2.89 \times 10^{-18}$ cm^2 $molecule^{-1}$, path length = 5 cm) was also used to determine the $[CS_2]$. The 214-nm line was produced by a Zn lamp and isolated by a band-pass filter (25% peak transmission at 211 nm, fwhm = 18 nm). The concentration of CS_2 was measured before it entered and after it left the reactor; the values are within experimental uncertainties and are approximately 10% greater than that determined from the flow rate. Considering the possible uncertainties associated with the values of the absorption cross section and path length, we used in the data analysis the CS_2 concentration determined from the flow rate.

Typical experimental conditions were as follows: total flow rate F_T = 2–18 STP cm^3 s^{-1}; total pressure P = 9–270 Torr; reaction temperature T = 246–298 K; $[H_2O_2] \simeq (3–12) \times 10^{13}$ molecules cm^{-3}; $[CS_2] = (0.2–12.4) \times 10^{16}$ molecules cm^{-3}; $[OH]_0 \simeq (0.8–4.0) \times 10^{11}$ molecules cm^{-3}; interval between two lasers t = 2 μs to 20 ms.

Results and Discussion

In Figure 1, a typical profile of the OH decay profile in the millisecond range of the OH + CS_2 reaction is plotted along with a single-exponential decay of OH when CS_2 was absent. The OH decay rate ~200 s^{-1} when CS_2 was absent was mainly due to the reaction of OH with H_2O_2, and the diffusion of OH from the viewing zone of the detector. The decay rate was approximately the same when CS_2 was present, whereas the "initial" (2 μs after photolysis) concentration of OH was much smaller than that in the absence of CS_2, even though care was taken to keep almost constant the amount of OH generated in both measurements. The decrease in the LIF signal of OH when CS_2 was present could not be satisfactorily explained by the rapid quenching of the fluorescence due to CS_2. When the detection period was moved forward into the microsecond range, typical double-exponential OH decay profiles were observed, as illustrated in Figure 2.

The reaction was studied with $[CS_2] \gg [OH]_0$ and under conditions in which the [OH] temporal profiles were clearly characterized by an initial rapid decay followed by a much slower decay toward the millisecond range of reaction time, as depicted in traces B and C of Figure 2. The two decay components of trace A in Figure 2 were not well separated and the derived rate coefficients exhibited greater uncertainties than those from traces B and C; hence experiments were carried out under conditions that produced temporal profiles such as traces B and C in Figure 2. To model the reactions, a simplified mechanism consists of the following reactions:

$$OH + CS_2 \xrightarrow{M} HOCS_2 \qquad (1f)$$

$$HOCS_2 \xrightarrow{M} OH + CS_2 \qquad (1r)$$

$$HOCS_2 \rightarrow \text{products other than OH} \qquad (3)$$

$$OH \rightarrow \text{products other than } HOCS_2 \qquad (4)$$

Reaction 3 includes diffusion of $HOCS_2$ from the probed volume and its possible loss due to homogeneous or heterogeneous processes. Reaction 4 takes into account reactions of OH with species other than CS_2 (mainly H_2O_2 and OH), the diffusion of OH away from the probed volume, and the possible bimolecular channel for the reaction

$$OH + CS_2 \rightarrow HS + OCS \text{ (or other products)} \qquad (5)$$

TABLE I: Summary of Decay Parameters of the [OH] Temporal Profile and Equilibrium Constants for the Reaction OH + $CS_2 \overset{M}{\leftrightarrow} HOCS_2$ in Helium at 269 K ≤ T ≤ 298 K[a]

expt no.	T/K	P/Torr	$[CS_2]/10^{14}$ [b]	$\alpha/10^3$ s^{-1}	$\beta/10^6$ s^{-2}	$\gamma/10^3$ s^{-1}	k_{slow}/s^{-1}	$x_{eq}/10^{-2}$	$K_c/10^{-17}$ [c]
1	298	23	281	10.17 ± 0.38	1.85 ± 0.08	7.39 ± 0.33	160 ● 4	79.1 ± 4.5	0.94 ± 0.26
2			345	12.28 ± 0.36	2.05 ± 0.07	9.16 ± 0.29	168 ± 3	75.3 ± 3.3	0.95 ± 0.17
3			518	15.82 ± 0.41	2.77 ± 0.08	10.82 ± 0.31	156 ± 4	68.8 ± 2.7	0.87 ± 0.12
4			667	17.58 ± 0.44	2.92 ± 0.09	10.93 ± 0.31	156 ± 4	62.4 ± 2.4	0.90 ± 0.10
5			784	18.44 ± 0.36	2.87 ± 0.07	10.86 ± 0.24	141 ± 4	59.1 ± 1.8	0.88 ± 0.08
6			917	22.71 ± 0.45	3.73 ± 0.10	12.22 ± 0.28	155 ± 4	55.2 ± 1.7	0.89 ± 0.08
7		69	400	43.02 ± 2.57	4.82 ± 0.33	32.16 ± 1.99	121 ± 6	74.9 ± 6.5	0.84 ± 0.29
8			653	37.43 ± 1.43	4.98 ± 0.22	23.82 ± 0.99	138 ± 6	63.7 ± 3.6	0.87 ± 0.14
9			1036	49.79 ± 2.50	7.97 ± 0.50	27.09 ± 1.49	137 ± 6	54.4 ± 4.1	0.81 ± 0.14
10		70	492	28.41 ± 1.22	4.04 ± 0.11	20.22 ± 0.93	142 ± 7	71.4 ± 4.5	0.82 ± 0.18
11			1237	39.12 ± 2.60	6.37 ± 1.08	19.44 ± 1.52	144 ± 35	49.7 ± 5.1	0.82 ± 0.17
12		49	230	18.47 ± 1.53	2.07 ± 0.17	15.28 ± 1.29	109 ± 2	83.1 ± 9.9	0.89 ± 0.62
13		154	228	49.21 ± 3.22	9.11 ± 0.61	41.89 ± 2.80	193 ± 4	85.4 ± 8.0	0.75 ± 0.48
14		204	237	57.87 ± 2.79	4.78 ± 0.24	49.29 ± 24.20	84 ± 1	85.3 ± 5.9	0.73 ± 0.34
15	283	69	260	18.34 ± 0.61	2.01 ± 0.07	12.17 ± 0.45	109 ± 3	66.6 ± 3.3	1.93 ± 0.30
16			475	25.92 ± 0.63	2.81 ± 0.09	14.19 ± 0.39	115 ± 4	54.8 ± 2.0	1.74 ± 0.17
17			640	32.71 ± 0.83	3.42 ± 0.17	13.78 ± 0.43	104 ± 8	42.1 ± 1.7	2.15 ± 0.19
18			1104	45.17 ± 1.38	6.77 ± 0.60	13.99 ± 0.58	126 ± 17	30.8 ± 1.6	2.03 ± 0.18
19	275	46	480	18.45 ± 0.50	2.18 ± 0.11	6.82 ± 0.24	123 ± 3	36.8 ± 1.7	3.58 ± 0.31
20			461	17.33 ± 0.38	3.26 ± 0.11	7.28 ± 0.21	195 ± 4	41.8 ± 1.5	3.02 ± 0.24
21			464	17.19 ± 0.28	5.56 ± 0.14	6.57 ± 0.15	300 ± 8	37.8 ± 1.1	3.55 ± 0.24
22	273	9	402	2.13 ± 0.52	0.32 ± 0.02	0.81 ± 0.04	164 ± 11	36.0 ± 2.5	4.42 ± 0.53
23			507	4.47 ± 0.97	0.68 ± 0.04	1.47 ± 0.06	145 ± 13	31.6 ± 1.6	4.26 ± 0.38
24	269	51	101	5.58 ± 0.16	0.70 ± 0.02	3.63 ± 0.12	133 ± 2	65.7 ± 2.9	5.20 ± 0.72
25			132	7.18 ± 0.20	0.79 ± 0.03	4.23 ± 0.14	109 ± 3	59.3 ± 2.6	5.21 ● 0.62
26			209	9.30 ± 0.36	1.53 ± 0.12	4.27 ± 0.22	163 ± 22	46.0 ± 3.0	5.67 ± 0.74
27			232	11.59 ± 0.17	1.43 ± 0.04	5.62 ± 0.10	130 ± 4	48.4 ± 1.2	4.59 ± 0.31
28			266	11.64 ± 0.21	1.24 ± 0.06	4.76 ± 0.12	117 ± 5	40.7 ± 1.3	5.47 ± 0.40
29			365	15.04 ± 0.37	2.61 ± 0.35	4.95 ± 0.21	132 ± 50	32.0 ± 2.0	5.70 ± 0.51
30			411	18.44 ± 0.35	2.52 ± 0.15	5.73 ± 0.16	111 ± 8	30.8 ± 1.0	5.46 ± 0.38
31			497	20.31 ± 0.32	1.93 ± 0.09	5.77 ± 0.13	95 ± 6	28.2 ± 0.8	5.12 ± 0.32
32		23	181	5.47 ± 0.09	0.90 ± 0.02	2.83 ± 0.06	167 ± 3	51.9 ± 1.4	5.13 ± 0.38
33		100	166	13.57 ± 0.26	1.35 ± 0.04	7.44 ± 0.17	102 ± 3	54.9 ± 1.6	4.96 ± 0.41
34		151	175	21.55 ± 0.36	2.09 ± 0.04	12.27 ± 0.22	95 ± 3	57.0 ± 1.4	4.32 ± 0.33
35		201	169	24.85 ± 0.49	2.74 ± 0.07	14.28 ± 0.30	115 ± 2	57.2 ± 1.7	4.38 ± 0.37

[a] The uncertainties represent one standard deviation. [b] In units of molecules cm^{-3}. [c] Determined from eqs 14 and 16, in units of cm^3 molecule^{-1}.

Provided that $[CS_2] \gg [OH]_0$, the differential equations can be solved to yield the time dependence of [OH]

$$[OH] = [OH]_0[(\gamma + \lambda_1)\exp(\lambda_1 t) - (\gamma + \lambda_2)\exp(\lambda_2 t)]/(\lambda_1 - \lambda_2) \quad (6)$$

in which

$$\lambda_1 = [(\alpha^2 - 4\beta)^{1/2} - \alpha]/2 < 0 \quad (7)$$

$$\lambda_2 = -[(\alpha^2 - 4\beta)^{1/2} + \alpha]/2 < 0 \quad (8)$$

$$\gamma = k_{1r} + k_3 \quad (9)$$

$$\alpha = k_{1f}[CS_2] + k_{1r} + k_3 + k_4 \quad (10)$$

$$\beta = k_{1f}k_3[CS_2] + k_{1r}k_4 + k_3k_4 \quad (11)$$

k_{1f} and k_{1r} are the apparent second-order and first-order rate coefficients for reactions 1f and 1r, respectively; k_3 and k_4 are the apparent first-order rate coefficients for reactions 3 and 4, respectively. The observed [OH] temporal profiles were fitted to eq 6 by using a nonlinear least-squares method to determine λ_1, λ_2, and γ. We found that accurate characterization of both the components of the [OH] profile for the rapid and the slow decays were required to determine precisely the parameters λ_1, λ_2, and γ from the fitting procedure. At least 80 data points spanning 2 μs to 20 ms were typically taken in each measurement of the temporal profile. The derived values α, β (from λ_1 and λ_2), and γ and the experimental conditions are listed in Tables I and II.

To derive k_{1f}, k_{1r}, k_3, and k_4 from the measured α, β, and γ using eqs 9–11 requires certain assumptions or approximations. However, a simple method could produce the equilibrium constant without explicit solution of k_{1f} and k_{1r}. When the experimental conditions were adjusted to produce an initial decay rate greater than 10^4 s^{-1} (with large $[CS_2]$ or under high pressure), and both k_3 and k_4 less than 200 s^{-1} (commonly with small $[H_2O_2]$ and $[OH]_0$), $\alpha^2 \gg \beta$; hence, $\lambda_1 \simeq -\beta/\alpha$ and $\lambda_2 \simeq -\alpha$. Because $|\lambda_1| \ll |\lambda_2|$, the component of slow decay obeys the condition

$$[OH] = [OH]_0(\gamma + \lambda_1)\exp(\lambda_1 t)/(\lambda_1 - \lambda_2) \quad (12)$$

Under such experimental conditions, the equilibrium was achieved in a brief period (on the order of α^{-1}); hence the slow decay may be described as

$$[OH] = [OH]_{eq}\exp(-k_{slow}t) \quad (13)$$

in which $[OH]_{eq}$ is the equilibrium concentration of OH if no loss of OH occurred. Comparison of eqs 12 and 13 leads to

$$x_{eq} = [OH]_{eq}/[OH]_0 = (\gamma + \lambda_1)/(\lambda_1 - \lambda_2) \quad (14)$$

$$k_{slow} = -\lambda_1 \simeq \beta/\alpha \quad (15)$$

hence the equilibrium constant K_c:

$$K_c = (1 - x_{eq})/x_{eq}[CS_2] \quad (16)$$

The component of the [OH] temporal profiles for the slow decay was also fitted with a single-exponential decay. The derived rate coefficients for this decay, k_{slow}, are also listed in Tables I and II. To avoid possible errors due to the uncertainties in k_{slow}, we derived x_{eq} from eq 14 rather than from the preexponential factor in eq 13 derived from the slow decay component; the values of x_{eq} and K_c derived by this method are also listed in Tables I and II. The assumptions made in the derivation of eq 12, $\alpha^2 \gg \beta$, can be easily verified from the data listed. The values of k_{slow} and β/α are similar in accordance with eq 15.

The equilibrium constant can also be derived from the rate coefficients of the forward and reverse reactions

$$K_c = k_{1f}/k_{1r} \quad (17)$$

hence x_{eq} can be expressed as

$$x_{eq} = [OH]_{eq}/[OH]_0 = k_{1r}/(k_{1f}[CS_2] + k_{1r}) \quad (18)$$

TABLE II: Summary of Decay Parameters of the [OH] Temporal Profile and Equilibrium Constants for the Reaction OH + $CS_2 \overset{M}{\leftrightarrow} HOCS_2$ at 246 K ≤ T ≤ 263 K[a]

expt no.	T/K	P/Torr	$[CS_2]/10^{14}$ [b]	$\alpha/10^3$ s^{-1}	$\beta/10^6$ s^{-2}	$\gamma/10^3$ s^{-1}	k_{slow}/s^{-1}	$x_{eq}/10^{-2}$	$K_c/10^{-17}$ [c]
36	263	28	239	8.04 ± 0.15	1.00 ± 0.04	2.86 ± 0.08	115 ± 5	35.1 ± 1.2	7.73 ± 0.55
37			414	12.20 ± 0.19	1.67 ± 0.11	3.13 ± 0.09	129 ± 11	25.1 ± 0.8	7.22 ± 0.48
38	259	27	121	3.92 ± 0.09	0.47 ± 0.02	1.91 ± 0.06	128 ± 6	48.6 ± 1.9	8.73 ± 0.80
39			365	10.70 ± 0.26	1.02 ± 0.10	2.29 ± 0.09	96 ± 9	20.9 ± 1.0	10.39 ± 0.83
40			705	27.30 ± 0.44	3.63 ± 1.15	3.88 ± 0.19	147 ± 85	13.9 ± 0.7	8.82 ± 0.70
41	253	76	165	9.81 ± 0.13	1.72 ± 0.07	3.07 ± 0.07	186 ± 6	30.5 ± 0.9	13.78 ± 0.90
42			300	15.64 ± 0.23	2.67 ± 0.21	2.86 ± 0.11	203 ± 9	17.6 ± 0.8	15.66 ± 1.13
43			387	21.24 ± 0.21	2.88 ± 0.22	3.06 ± 0.09	149 ± 11	14.0 ± 0.5	15.93 ± 1.00
44			540	30.19 ± 0.43	4.90 ± 0.76	3.77 ± 0.16	183 ± 34	12.1 ± 0.6	13.48 ± 0.98
45			540	30.19 ± 0.43	4.90 ± 0.76	3.77 ± 0.16	183 ± 34	12.1 ± 0.6	13.48 ± 0.98
45	249	52	18	2.01 ± 0.06	0.22 ± 0.01	1.40 ± 0.05	113 ± 1	72.0 ± 3.5	21.51 ± 1.82
46			48	2.95 ± 0.05	0.33 ± 0.01	1.34 ± 0.03	117 ± 2	45.2 ± 1.3	25.51 ± 1.82
47			67	4.21 ± 0.07	0.41 ± 0.01	1.45 ± 0.04	102 ± 2	33.7 ± 1.1	29.26 ± 2.04
48			72	4.28 ± 0.06	0.48 ± 0.01	1.52 ± 0.03	115 ± 2	34.7 ± 1.0	26.25 ± 1.72
49			93	5.17 ± 0.07	0.53 ± 0.03	1.44 ± 0.04	110 ± 4	26.8 ± 0.8	29.32 ± 1.88
50			232	13.76 ± 0.22	1.05 ± 0.31	1.81 ± 0.09	84 ± 31	12.7 ± 0.7	29.54 ± 2.40
51			336	19.96 ± 0.18	0.86 ± 0.17	2.26 ± 0.05	40 ± 13	11.1 ± 0.3	23.75 ± 1.38
52		54	230	13.62 ± 0.24	0.77 ± 0.10	2.46 ± 0.08	56 ± 10	17.8 ± 0.7	20.04 ± 1.38
53		104	90	7.97 ± 0.12	0.91 ± 0.04	2.17 ± 0.50	105 ± 4	26.6 ± 0.8	30.58 ± 1.95
54		152	104	11.55 ± 0.17	1.28 ± 0.05	2.94 ± 0.07	111 ± 7	25.0 ± 0.7	28.84 ± 1.80
55		203	99	14.54 ± 0.27	1.64 ± 0.09	3.72 ± 0.10	103 ± 6	25.2 ± 0.9	30.01 ± 2.02
56		207	95	16.35 ± 0.34	4.84 ± 0.26	4.64 ± 0.17	301 ± 15	27.6 ± 1.2	27.63 ± 2.16
57	246	32	25	2.23 ± 0.06	0.15 ± 0.00	1.32 ± 0.04	74 ± 1	59.7 ± 2.4	26.85 ± 3.02
58			90	4.79 ± 0.05	0.30 ± 0.02	1.23 ± 0.03	65 ± 5	25.0 ± 0.6	33.32 ± 2.00
59			121	6.67 ± 0.09	0.43 ± 0.04	1.36 ± 0.04	71 ± 8	19.8 ± 0.7	33.58 ± 2.18
60			138	7.80 ± 0.10	0.46 ± 0.05	1.38 ± 0.04	74 ± 8	17.2 ± 0.6	34.94 ± 2.27
61			148	8.71 ± 0.14	0.70 ± 0.08	1.41 ± 0.05	92 ± 9	15.5 ± 5.6	36.91 ± 2.58
62			193	10.77 ± 0.22	0.91 ± 0.23	1.68 ± 0.09	114 ± 27	15.0 ± 0.9	29.23 ± 5.57
63			249	15.16 ± 0.22	1.28 ± 0.23	2.02 ± 0.79	99 ± 21	12.9 ± 0.6	26.98 ± 1.92

[a] The experiments were carried out in He except that those at 246 K were in Ar. The uncertainties represent one standard deviation. [b] In units of molecules cm^{-3}. [c] Determined from eqs 14 and 16, in units of cm^3 molecule^{-1}.

Because $(k_3 + k_4)$ are typically less than 5% of $(k_{1r} + k_{1f}[CS_2])$ under our experimental conditions, eqs 10, 11, and 18 yield

$$\beta/\alpha \simeq x_{eq}k_4 + (1 - x_{eq})k_3 \qquad (19)$$

This equation states that the rate coefficient for the decay of the slow component is determined by a weighted average of the rate coefficients for the loss of OH and $HOCS_2$.

The upper limit for the rate coefficient of reaction 5 has previously been determined to be less than 2×10^{-15} cm^3 molecule^{-1} s^{-1}.[15] In our experiments, k_{slow} was constant for $[CS_2] = (2.8–9.2) \times 10^{16}$ molecules cm^{-3} at 298 K; hence an upper limit of $k_5 \leq 1 \times 10^{-16}$ cm^3 molecule^{-1} s^{-1} was estimated. For the analysis, the rate coefficient k_4 for the loss of OH was therefore determined from the [OH] decay in the absence of CS_2. Under our experimental conditions, $k_4 < 200$ s^{-1} in most cases. Experimentally this condition was achieved through the use of a small concentration of H_2O_2 ($[H_2O_2] < 1.2 \times 10^{14}$ molecules cm^{-3}) and production of $[OH]_0 < 4 \times 10^{11}$ molecules cm^{-3}, so that the reaction

$$OH + H_2O_2 \rightarrow HO_2 + H_2O \qquad (20)$$

in which $k_{20} = 1.7 \times 10^{-12}$ cm^3 molecule^{-1} s^{-1},[17] was the major contribution to the loss of OH in the slow decay. The reaction

$$OH + OH \rightarrow \text{products} \qquad (21)$$

in which $k_{21} = 1.9 \times 10^{-12}$ cm^3 molecule^{-1} s^{-1},[18] was unimportant because $[OH]_0 < 4 \times 10^{11}$ molecules cm^{-3}.

With the values of k_4 determined experimentally from the OH decay in the absence of CS_2, the rate coefficients k_{1f}, k_{1r}, and k_3 were calculated from eqs 9–11. The rate coefficients thus obtained and the equilibrium constants K_c (calculated from eq 17) are listed in Tables III and IV. The values of k_3 were also determined from eq 19; they are in excellent agreement with those derived from eqs 9–11.

It was found that values of k_{1f} and k_{1r} are insensitive to the values of k_3 and k_4 under our experimental conditions. For a typical temporal profile, an increase of k_3 by 200 s^{-1} changes k_{1f}, k_{1r}, and K_c by only 2, −2, and 4%, respectively. Similarly, an increase of k_4 by 200 s^{-1} changes k_{1f}, k_{1r}, and K_c by only −2, 2, and −4%, respectively. The error in the measurement of [OH] due to the error in the subtraction of the scattered light from the LIF signal is estimated to be ~2% of $[OH]_0$. If the entire [OH] temporal profile is shifted upward by 0.02 $[OH]_0$, the derived values of k_{1f}, k_{1r}, and K_c decrease by ~8, 2, and 6%, respectively. Uncertainty in the $[OH]_0$ measurement due to the instability of the LIF signal and the error in the timing of the two lasers is estimated to be approximately 3%. If the entire [OH] temporal profile is multiplied by 1.03, the derived values of k_{1f}, k_{1r}, and K_c decrease by ~8, 4, and 4%, respectively. The systematic errors in the measurements of $[CS_2]$ were about 3%. The standard errors of the rate coefficients in the nonlinear fitting were typically ±8%. Therefore, the 95% confidence limits for the measurements of k_{1f}, k_{1r}, and K_c are estimated to be approximately ±15, ±12, and ±20%, respectively.

As listed in Tables I–IV, the K_c values derived from both methods (eqs 14 and 17) are in excellent agreement. We found no dependence of K_c on pressure or $[CS_2]$; for this reason the K_c values were averaged at each temperature. The data were weighted by the inverse of their variance. The weighted averages of K_c from both methods are listed in Table V. The discrepancies are within 6%; hence the averaged value of K_c from the two methods is reported, as listed in Table V. The equilibrium constant K_p (in units of atm^{-1}) can be calculated from

$$K_p = K_c/RT = 7.34 \times 10^{21}K_c/T \qquad (22)$$

in which K_c is in units of cm^3 molecule^{-1}. The K_p values are also listed in Table V, with uncertainties representing one standard error. The values reported by Hynes et al. are approximately 1.6

(17) Keyser, L. F. *J. Phys. Chem.* **1980**, *84*, 1659.
(18) DeMore, W. B.; Molina, M. J.; Sander, S. P.; Hampson, R. F.; Kurylo, M. J.; Golden, D. M.; Howard, C. J.; Ravishankara, A. R. "Chemical Kinetics and Photochemical Data for Use in Stratospheric Modeling"; Publication 87-41, Jet Propulsion Laboratory, Pasadena, CA, 1987.

TABLE III: Summary of Rate Coefficients and Equilibrium Constants at 269 K ≤ T ≤ 298 K[a]

expt no.	T/K	P/Torr	$[CS_2]/10^{14}$ [b]	k_4/s^{-1}	k_3/s^{-1}	$k_{1f}/10^{-13}$ [c]	$k_{1r}/10^3\ s^{-1}$	$K_c/10^{-17}$ [d]
	298	23	281	208 ± 4	98 ± 58	0.72 ± 0.18	7.83 ± 0.33	0.92 ± 0.24
2			345		48 ± 34	0.84 ± 0.14	9.11 ± 0.29	0.92 ± 0.16
3			518		108 ± 27	0.92 ± 0.11	10.71 ± 0.31	0.86 ± 0.11
4			667		100 ± 21	0.97 ± 0.09	10.83 ± 0.31	0.89 ± 0.09
5			784		83 ± 15	0.94 ± 0.07	10.78 ± 0.24	0.87 ± 0.07
6			917		122 ± 17	1.06 ± 0.08	12.10 ± 0.28	0.88 ± 0.07
7		69	400		195 ± 70	2.69 ± 0.82	31.96 ± 1.99	0.84 ± 0.26
8			653		220 ± 37	2.07 ± 0.29	23.60 ± 0.99	0.88 ± 0.13
9			1036		251 ± 43	2.18 ± 0.30	26.84 ± 1.49	0.81 ± 0.12
10		70	492		180 ± 49	1.64 ± 0.32	20.04 ± 0.93	0.82 ± 0.17
11			1237		199 ± 66	1.58 ± 0.26	19.24 ± 1.53	0.82 ± 0.15
12		49	230	118 ± 3	86 ± 95	1.34 ± 0.88	15.19 ± 1.29	0.88 ± 0.58
13		154	228	202 ± 6	91 ± 133	3.13 ± 1.88	41.80 ± 2.80	0.75 ± 0.45
14		204	237	79 ± 3	106 ± 61	3.59 ± 1.57	49.18 ± 2.42	0.73 ± 0.32
15	283	69	260	80 ± 2	170 ± 28	2.34 ± 0.31	12.00 ± 0.45	1.95 ± 0.27
16			475		144 ± 16	2.45 ± 0.20	14.05 ± 0.39	1.75 ± 0.15
17			640		123 ± 14	2.94 ± 0.21	13.66 ± 0.43	2.16 ± 0.17
18			1104		182 ± 25	2.81 ± 0.20	13.80 ± 0.58	2.04 ± 0.17
19	275	46	480	79 ± 2	143 ± 16	2.41 ± 0.17	6.67 ± 0.24	3.61 ± 0.28
20			461	221 ± 6	168 ± 19	2.14 ± 0.14	7.11 ± 0.21	3.01 ± 0.22
21			464	394 ± 15	290 ± 29	2.20 ± 0.13	6.28 ± 0.15	3.51 ± 0.22
22	273	9	402	213 ± 8	134 ± 23	2.75 ± 0.22	0.68 ± 0.05	4.05 ± 0.43
23			507		130 ± 19	5.49 ± 0.36	1.34 ± 0.06	4.10 ± 0.33
24	269	51	101	184 ± 3	21 ± 19	1.77 ± 0.22	3.60 ± 0.12	4.90 ± 0.62
25			132	144 ± 2	64 ± 15	2.12 ± 0.12	4.17 ± 0.14	5.09 ± 0.54
26			209	168 ± 5	168 ± 32	2.33 ± 0.23	4.11 ± 0.22	5.67 ± 0.64
27			232	184 ± 3	69 ± 10	2.50 ± 0.15	5.55 ± 0.10	4.49 ± 0.29
28			266		55 ± 11	2.52 ± 0.16	4.71 ± 0.12	5.35 ± 0.36
29			365	168 ± 5	180 ± 38	2.72 ± 0.18	4.77 ± 0.21	5.71 ± 0.45
30			411		117 ± 15	3.04 ± 0.18	5.62 ± 0.16	5.41 ± 0.35
31			497		60 ± 8	2.89 ± 0.16	5.71 ± 0.13	5.05 ± 0.30
32		23	181	253 ± 3	77 ± 13	1.32 ± 0.09	2.76 ± 0.06	4.79 ± 0.33
33		100	166	107 ± 2	92 ± 11	3.64 ± 0.26	7.34 ± 0.17	4.95 ± 0.37
34		151	175		85 ± 9	5.25 ± 0.36	12.19 ± 0.22	4.31 ± 0.30
35		201	169		116 ± 13	6.21 ± 0.46	14.17 ± 0.30	4.38 ± 0.34

[a] The experiments were carried out in helium. The uncertainties represent one standard deviation. [b] In units of molecules cm^{-3}. [c] In units of cm^3 $molecule^{-1}$ s^{-1}. [d] Determined from eq 17, in units of cm^3 $molecule^{-1}$.

TABLE IV: Summary of Rate Coefficients and Equilibrium Constants at 246 K ≤ T ≤ 263 K[a]

expt no.	T/K	P/Torr	$[CS_2]/10^{14}$ [b]	k_4/s^{-1}	k_3/s^{-1}	$k_{1f}/10^{-13}$ [c]	$k_{1r}/10^3\ s^{-1}$	$K_c/10^{-17}$ [d]
36	263	28	239	117 ± 3	130 ± 13	2.12 ± 0.13	2.73 ± 0.08	7.76 ± 0.51
37			414		145 ± 17	2.16 ± 0.12	2.98 ± 0.09	7.25 ± 0.45
38	259	27	121	88 ± 2	156 ± 17	1.59 ± 0.12	1.75 ± 0.06	9.05 ± 0.74
39			365		98 ± 15	2.28 ± 0.14	2.19 ± 0.10	10.41 ± 0.77
40			705		141 ± 51	3.31 ± 0.18	3.74 ± 0.19	8.85 ± 0.66
41	253	76	165	198 ± 9	170 ± 17	3.97 ± 0.22	2.90 ± 0.08	13.69 ± 0.84
42			300		168 ± 21	4.20 ± 0.23	2.69 ± 0.11	15.59 ± 1.05
43			387		126 ± 16	4.65 ± 0.24	2.94 ± 0.09	15.82 ± 0.95
44			540	140 ± 4	166 ± 31	4.87 ± 0.26	3.60 ± 0.16	13.51 ± 0.94
45	249	52	18	118 ± 2	103 ± 26	2.72 ± 0.45	1.29 ± 0.06	21.05 ± 3.59
46			48		114 ± 11	3.12 ± 0.19	1.23 ± 0.03	25.42 ± 1.69
47			67		89 ± 9	3.92 ± 0.23	1.36 ± 0.04	28.82 ± 1.87
48			72		111 ± 10	3.69 ± 0.21	1.41 ± 0.03	26.15 ± 1.62
49			93		98 ± 10	3.89 ± 0.21	1.34 ± 0.04	29.08 ± 1.76
50			232		70 ± 27	5.10 ± 0.28	1.74 ± 0.09	29.33 ± 2.24
51			336		34 ± 10	5.23 ± 0.27	2.22 ± 0.06	23.55 ± 1.34
52		54	230	115 ± 3	44 ± 9	4.80 ± 0.26	2.24 ± 0.08	19.83 ± 1.29
53		104	90	165 ± 3	97 ± 9	6.24 ± 0.35	2.08 ± 0.05	30.05 ± 1.82
54		152	104		94 ± 9	8.12 ± 0.44	2.85 ± 0.07	28.48 ± 1.70
55		203	99		97 ± 11	10.76 ± 0.61	3.62 ± 0.10	29.73 ± 1.88
56		270	95	423 ± 11	255 ± 31	11.87 ± 0.72	4.39 ± 0.17	27.05 ± 1.93
57	246	32	25	70 ± 1	73 ± 10	3.36 ± 0.32	1.25 ± 0.04	26.93 ± 2.73
58			90		61 ± 7	3.88 ± 0.21	1.17 ± 0.03	33.20 ± 1.91
59			121		64 ± 9	4.34 ± 0.23	1.29 ± 0.04	33.53 ± 2.06
60			138		58 ± 9	4.61 ± 0.24	1.32 ± 0.04	34.83 ± 2.16
61			148		83 ± 12	4.89 ± 0.26	1.32 ± 0.05	37.03 ± 2.45
62			193		88 ± 26	4.67 ± 0.26	1.59 ± 0.09	29.33 ± 2.39
63			249		87 ± 18	5.24 ± 0.28	1.94 ± 0.08	27.04 ± 1.83

[a] The experiments were carried out in He except that those at 246 K were in Ar. The uncertainties represent one standard deviation. [b] In units of molecules cm^{-3}. [c] In units of cm^3 $molecule^{-1}$ s^{-1}. [d] Determined from eq 17, in units of cm^3 $molecule^{-1}$.

times our values near 298 K, and 1.3 times near 250 K. The values determined by Ravishankara and co-workers are approximately twice our values throughout the temperature range 249–298 K; there is no apparent reason for these discrepancies. It is not

TABLE V: Summary of Equilibrium Constants at 246 K ≤ T ≤ 298 K[a]

T/K	M	$K_c/10^{-17}$ cm^3 molecule^{-1} from eq 14	$K_c/10^{-17}$ cm^3 molecule^{-1} from eq 17	av $K_c/10^{-17}$ cm^3 molecule^{-1}	$K_p/10^2$ atm^{-1}
298	He	0.874 ± 0.039	0.866 ± 0.033	0.869 ± 0.036	2.14 ± 0.09
283	He	1.95 ± 0.19	1.96 ± 0.19	1.96 ± 0.18	5.08 ± 0.46
275	He	3.35 ± 0.32	3.34 ± 0.32	3.35 ± 0.29	8.94 ± 0.77
273	He	4.31 ± 0.11	4.08 ± 0.11	4.18 ± 0.15	11.24 ± 0.39
269	He	4.97 ± 0.47	4.88 ± 0.44	4.92 ± 0.45	13.43 ± 1.22
263	He	7.44 ± 0.36	7.47 ± 0.36	7.46 ± 0.29	20.82 ± 0.82
259	He	9.24 ± 0.89	9.37 ± 0.82	9.31 ± 0.77	26.39 ± 2.18
253	He	14.60 ± 1.25	41.54 ± 1.21	14.57 ± 1.14	42.27 ± 3.31
249	He	26.31 ± 3.66	26.07 ± 3.61	26.18 ± 3.55	77.19 ± 10.46
246	Ar	31.72 ± 3.86	31.67 ± 3.82	31.69 ± 3.69	94.58 ± 11.01

[a] The uncertainties represent one standard deviation.

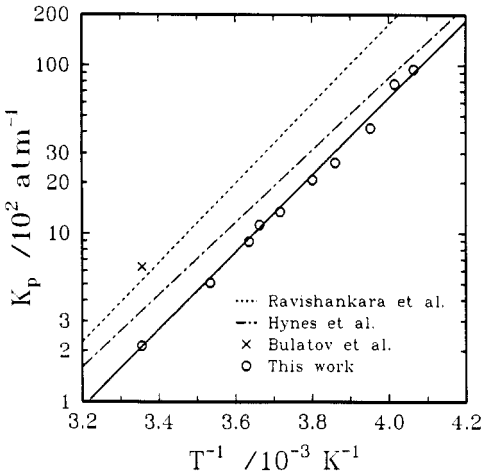

Figure 3. van't Hoff plot for the OH + CS_2 ↔ $HOCS_2$ equilibrium.

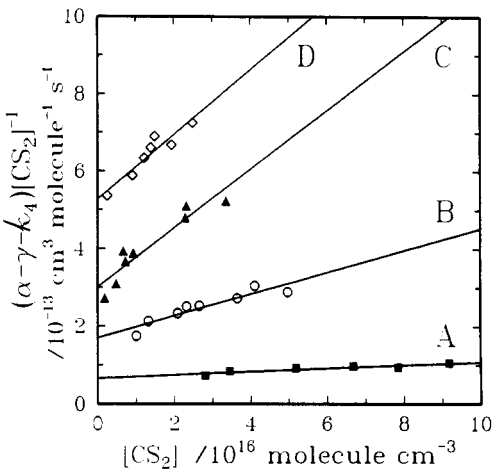

Figure 4. $k^{III}_{CS_2}$ measurement in the $(\alpha - \gamma - k_4)[CS_2]^{-1}$ vs $[CS_2]$ plot. (A) 298 K, P_{He} = 23 Torr (1–6); (B) 269 K, P_{He} = 51 Torr (24–31); (C) 249 K, P_{He} = 52 Torr (45–52); (D) 246 K, P_{Ar} = 32 Torr (57–63). The numbers in parentheses correspond to the experiment numbers listed in Tables I–IV. The origin for D has been displaced vertically by 2 × 10^{-13} cm^3 molecule^{-1} s^{-1}.

possible to compare the decay parameters in these studies because $[CS_2]$, k_3, and k_4 were not listed in previous studies. Although Hynes et al. assumed $k_3 = 0$ in their study and Ravishankara and co-workers set either k_3 or k_4 constant in their analysis depending on experimental conditions, the differences in the data analysis cannot account for all the discrepancies. More data points covering a more extended period of reaction were also obtained in this study to characterize fully the temporal profile of [OH]. It was found that the maximum intervals of delay for the [OH] temporal profile should be greater than $4t_{eq}$, in which t_{eq} is the time required for [OH] to reach $x_{eq}[OH]_0$, so that consistent rate coefficients were derived from the profile. If the maximum delay is reduced to $2t_{eq}$, the values of k_{1f}, k_{1r}, and K_c increase by ~−2, −12, and 10%, respectively, for a typical decay profile. The maximum error in the measurements of CS_2 concentration among these studies should be less than 10%, too small to account for all the discrepancies. The $[OH]_0$ employed in this work is the smallest in any investigations, as indicated from the small values of k_4; other studies reported $k_4 > 400$ s^{-1}. Presumably the error due to unknown secondary reactions is least when $[OH]_0$ is smallest.

The van't Hoff plot, K_p vs T^{-1}, is shown in Figure 3. The K_p value at 246 K was determined in Ar. The K_p values seem independent of the third body, consistent with other studies. The results from previous studies are also indicated by dashed lines. A fit of the averaged K_p to the van't Hoff equation by least squares yielded $\Delta H = -(43.9 \pm 1.3)$ kJ mol^{-1} and $\Delta S = -(102.9 \pm 4.2)$ J K^{-1} mol^{-1} for reaction 1f; the uncertainties represent one standard deviation. The excellent linearity in Figure 3 also indicates that ΔH is independent of temperature within the range of our study. Considering the errors discussed previously, we estimated the 95% confidence limits of our determinations in ΔH and ΔS to be ±12 and ±15%, respectively; hence $\Delta H° = -(43.9 \pm 5.3)$ kJ mol^{-1} and $\Delta S° = -(102.9 \pm 15.4)$ J K^{-1} mol^{-1}. The values of $\Delta H°$ determined in this work are in excellent agreement with those reported by Hynes et al. (−41.4 ± 5.0 kJ mol^{-1}) and by Ravishankara and co-workers, (−45.6 ± 4.2 kJ mol^{-1}). Our $\Delta H°$ value implies $\Delta H_f°(HOCS_2)$ = 112 ± 5 kJ mol^{-1}.[19]

The $\Delta S°$ value is also in excellent agreement with the value $\Delta S° = -100.5 \pm 18.4$ J K^{-1} mol^{-1} reported by Ravishankara and co-workers. Although Hynes et al. did not report ΔS, a value −89.5 J K^{-1} mol^{-1} was derived from their data, 13.4 J mol^{-1} K^{-1} more positive than our result. These values indicate that $S°_{298}(HOCS_2) \geq 318.8$ J K^{-1} mol^{-1}.[19] We used $S°_{298}(CS_2) = 238.0$ J K^{-1} mol^{-1} to estimate $S°_{298}$ by considering various contributions to $S°_{298}(HOCS_2)$ due to the changes in mass, vibrational frequencies, moment of inertia, symmetry, and number of isomers.[20] Although the structure and the vibrational frequencies of the possible isomers of $HOCS_2$ are unknown, we found that the straight-chain isomer, HOSCS, is favored for such a large value of $S°_{298}$ according to our estimate. Further information, possibly the IR absorption spectrum of the adduct, is needed in order to determine the structure of the adduct. The straight-chain structure of the adduct is also consistent with the results of the reaction mechanism studied by Ravishankara and co-workers.[21]

Under our experimental conditions, the apparent second-order rate coefficient of reaction 1f is expressed as

$$k_{1f} = k^{III}_{He}[He] + k^{III}_{CS_2}[CS_2] + k^{II}_{int} \qquad (23)$$

in which k^{III}_{He} and $k^{III}_{CS_2}$ are the termolecular rate coefficients of reaction 1f for M = He and CS_2, respectively; k^{II}_{int}, the pres-

(19) $\Delta H_f°(OH) = 38.987 \pm 1.21$ kJ mol^{-1}, $\Delta H_f°(CS_2) = 116.943 \pm 0.84$ kJ mol^{-1}, $S°(OH) = 183.718 \pm 0.04$ J mol^{-1} K^{-1}, and $S°(CS_2) = 237.977 \pm 0.08$ J mol^{-1} K^{-1} were taken from *JANAF Thermochemical Tables*, 3rd ed. (*J. Phys. Chem. Ref. Data* **1985**, *14*).

(20) Benson, S. W. *Thermochemical Kinetics*, 2nd ed.; Wiley: New York, 1976.

(21) Lovejoy, E. R.; Murrells, T. P.; Ravishankara, A. R.; Howard, C. J. *J. Phys. Chem.* **1990**, *94*, 2386.

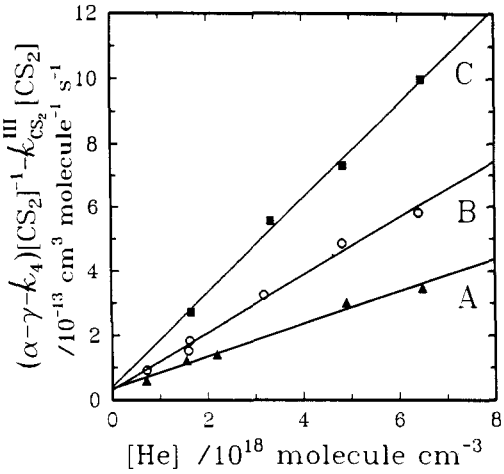

Figure 5. k^{III}_{He} measurement in the $(\alpha - \gamma - k_4)[CS_2]^{-1} - k^{III}_{CS_2}[CS_2]$ vs [He] plot. (A) 298 K (1, 10, 12–14); (B) 269 K (24, 25, 32–35); (C) 249 K (46, 53–55). The numbers in parentheses correspond to the experiment numbers listed in Tables I–IV.

TABLE VI: Rate Coefficients for the Forward and Reverse Reaction $OH + CS_2 \overset{M}{\leftrightarrows} HOCS_2$[a]

T/K	$k^{III}_{CS_2}/10^{-31}$ [b]	$k^{R}_{CS_2}/10^{-15}$ [c]	$k^{III}_{He}/10^{-31}$ [b]	$k^{R}_{He}/10^{-15}$ [c]
298	4.28 ± 0.90	57.9 ± 11.0	0.504 ± 0.034	7.36 ± 0.40
269	28.3 ± 4.6	46.8 ± 13.5	0.891 ± 0.042	2.14 ± 0.12
249	76.0 ± 11.3	35.9 ± 7.5	1.47 ± 0.07	0.46 ± 0.01
246	83.7 ± 13.2	31.9 ± 8.0		

[a] The uncertainties represent one standard deviation. [b] In units of cm^6 molecule^{-2} s^{-1}. [c] In units of cm^3 molecule^{-1} s^{-1}.

sure-independent part of k_{1f}, may be due to the heterogeneous reaction or the effect caused by the falloff. The contribution of $M = CS_2$ to the termolecular reaction is significant, especially at greater concentrations of CS_2. Thus, eq 10 becomes

$$\alpha = k^{III}_{CS_2}[CS_2]^2 + (k^{III}_{He}[He] + k^{II}_{int})[CS_2] + k_{1r} + k_3 + k_4 \quad (24)$$

or

$$(\alpha - \gamma - k_4)[CS_2]^{-1} = k^{III}_{CS_2}[CS_2] + k^{III}_{He}[He] + k^{II}_{int} \quad (25)$$

The plot of $(\alpha - \gamma - k_4)[CS_2]^{-1}$ vs $[CS_2]$ at constant pressure and temperature produces a straight line with a slope equal to $k^{III}_{CS_2}$; such plots at various temperatures are shown in Figure 4. The values of $k^{III}_{CS_2}$ fitted by linear least squares are summarized in Table VI. At 298 K, $k^{III}_{CS_2} = 4.28 \times 10^{-31}$ cm^6 molecule^{-2} s^{-1}. The experiments were also carried out in Ar at 246 K. The determined value of $k^{III}_{CS_2}$ was unaffected by the presence of Ar.

Similarly, in a separate set of experiments with relatively small $[CS_2]$ at various partial pressures of helium, the plot of $(\alpha - \gamma - k_4)[CS_2]^{-1} - k^{III}_{CS_2}[CS_2]$ vs [He] yielded a straight line with a slope equal to k^{III}_{He}. Figure 5 illustrates such plots at 249, 269, and 298 K. The good linearity indicates that reaction 1f is still in the third-order region at pressures less than 200 Torr. The values of k^{III}_{He} fitted by least squares are also summarized in Table VI. At 298 K, $k^{III}_{He} = 5.04 \times 10^{-32}$ cm^6 molecule^{-2} s^{-1}; the ratio of $k^{III}_{CS_2}$ to k^{III}_{He} is approximately 9, a reasonable value in comparison to $k^{III}_{SO_2}:k^{III}_{He} \simeq 11:1$ in the reaction[22-24]

$$OH + SO_2 \xrightarrow{M} HOSO_2 \quad (26)$$

The apparent second-order rate coefficient k_{1r} for the reverse reaction is expressed as

$$k_{1r} = k^{R}_{He}[He] + k^{R}_{CS_2}[CS_2] + k^{R}_{int} \quad (27)$$

(22) Lee, Y.-Y.; Kao, W.-C.; Lee, Y.-P. *J. Phys. Chem.* **1990**, *94*, 4535.
(23) Leu, M.-T. *J. Phys. Chem.* **1982**, *86*, 4558.
(24) Martin, D.; Jourdain, J. L.; Le Bras, G. *J. Phys. Chem.* **1986**, *90*, 4143.

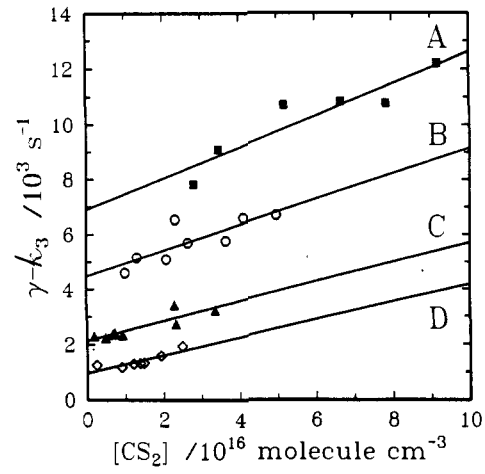

Figure 6. $k^{R}_{CS_2}$ measurement in the $(\gamma - k_3)$ vs $[CS_2]$ plot. (A) 298 K, P_{He} = 23 Torr (1–6); (B) 269 K, P_{He} = 51 Torr (24–31); (C) 249 K, P_{He} = 52 Torr (45–52); (D) 246 K, P_{Ar} = 32 Torr (57–63). The numbers in parentheses correspond to the experiment numbers listed in Tables I–IV. The origins for B and C have been displaced vertically by 1 × 10^{-3} s^{-1}.

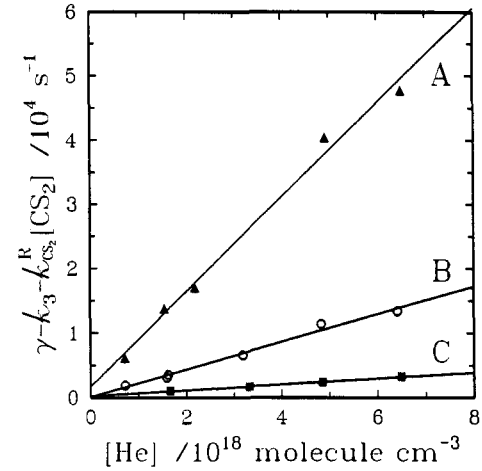

Figure 7. k^{R}_{He} measurement in the $(\gamma - k_3 - k^{R}_{CS_2}[CS_2])$ vs [He] plot. (A) 298 K (1, 10, 12–14); (B) 269 K (24, 25, 32–35); (C) 249 K (46, 53–55). The numbers in parentheses correspond to the experiment numbers listed in Tables I–IV.

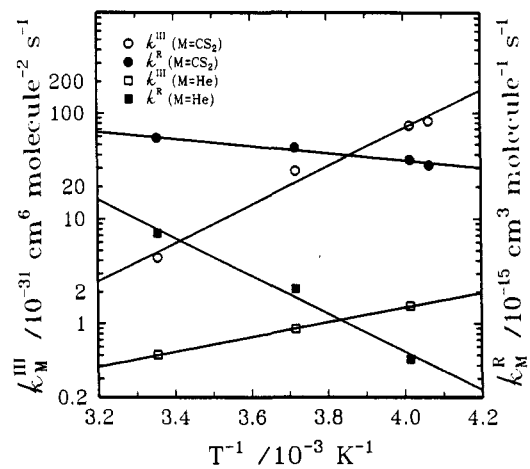

Figure 8. Arrhenius plot of $k^{III}_{CS_2}$, k^{III}_{He}, $k^{R}_{CS_2}$, and k^{R}_{He}. The ordinate for $k^{R}_{CS_2}$ and k^{R}_{He} is shown on the right.

in which k^{R}_{He} and $k^{R}_{CS_2}$ are the bimolecular rate coefficient for the reverse reaction 1r; k^{R}_{int} is the pressure-independent part of k_{1r}. Therefore, eq 9 becomes

$$(\gamma - k_3) = k^{R}_{CS_2}[CS_2] + k^{R}_{He}[He] + k^{R}_{int} \quad (28)$$

The plots of $(\gamma - k_3)$ vs $[CS_2]$ at constant [He] are shown in Figure

6. The slope fitted by linear least squares yielded values of $k^R_{CS_2}$. Similarly, the coefficient k^R_{He} was determined from the plots of $(\gamma - k_3 - k^R_{CS_2}[CS_2])$ vs [He], as illustrated in Figure 7. The values k^R_{He} and $k^R_{CS_2}$ are also listed in Table VI. At 298 K, $k^R_{CS_2} = 5.79 \times 10^{-14}$ cm^3 molecule^{-1} s^{-1} and $k^R_{He} = 7.36 \times 10^{-15}$ cm^3 molecule^{-1} s^{-1}.

The rate coefficients determined by fitting the double-exponential decay plot are not as accurate as those determined from a simple exponential decay. The uncertainties in the measurements of $k^R_{CS_2}$ and $k^{III}_{CS_2}$ are greater than those of k^R_{He} and k^{III}_{He} due to the limited range of $[CS_2]$ that can be used to produce good plots of [OH] decay. We estimate the 95% confidence limits to be ±25% for $k^{III}_{CS_2}$ and $k^R_{CS_2}$, and ±20% for k^{III}_{He} and k^R_{He}.

The values of k^{III}_{He}, $k^{III}_{CS_2}$, k^R_{He}, and $k^R_{CS_2}$ are shown in an Arrhenius plot, Figure 8. These rate coefficients were fitted to lead to activation energies $E_a = -13.4 \pm 0.3$, 34.6 ± 4.1, -34.7 ± 3.2, and 6.7 ± 0.8 kJ mol^{-1} for k^{III}_{He}, k^R_{He}, $k^{III}_{CS_2}$, and $k^R_{CS_2}$, respectively; the uncertainties represent one standard deviation. The 95% confidence limits for the measurements of E_a are estimated to be ~±25%. The temperature dependence of $k^{III}_{CS_2}$ and $k^R_{CS_2}$ yield $\Delta H°$ for the title reaction, -49.7 ± 10.4 kJ mol^{-1}, in agreement with that determined from the van't Hoff plot. The $\Delta H°$ derived from k^{III}_{He} and k^R_{He} is slightly greater because k^{III}_{He} and k^R_{He} were determined at only three temperatures; and the data at 249 K gave a relatively large value of K_c. The $-E_a$ value for $k^{III}_{CS_2}$ is approximately 20 kJ mol^{-1} greater than that for k^{III}_{He}, presumably because the deactivation by the polyatomic CS_2 molecules is relatively more efficient at low temperatures.

In summary, the reaction between OH and CS_2 has been studied by means of the laser-photolysis/laser-induced-fluorescence technique. The equilibrium constants were determined to be smaller than those from previous studies, whereas the value of $\Delta H°$ agrees well. The rate coefficients for the forward and reverse reaction (for M = He and CS_2) have been reported for the first time; their dependence on temperature has also been studied.

Acknowledgment. This research is supported by the National Science Council of the Republic of China. We are grateful to Dr. A. R. Ravishankara for communicating results to us before publication.

Influence of Solute–Solvent Asymmetry upon the Behavior of Dilute Supercritical Mixtures

Irena B. Petsche and Pablo G. Debenedetti*

Department of Chemical Engineering, Princeton University, Princeton, New Jersey 08544-5263
(Received: May 3, 1990)

Infinitely dilute supercritical mixtures may be classified into three categories: attractive, weakly attractive, and repulsive, according to the sign of the solute's partial molar properties, and of the excess number of solvent molecules surrounding a given solute molecule. These quantities are arbitrarily large near the solvent's critical point. Their sign is determined by differences in size, energy, and shape between solute and solvent (molecular asymmetry). The attractive or repulsive character of a van der Waals mixture is determined by the ratio of solute to solvent specific energies, referred to the respective molecular volumes. For a lattice-gas mixture with constant cell size, the boundaries between the three regimes are a function of chain length ratio, segment energy ratio, and solvent length. A simplified perturbed hard chain model predicts van der Waals-like behavior in the limit of unit chain length, and lattice-like behavior in the limit of constant segment size. The classification into attractive and repulsive behavior can also be expressed in terms of slopes of critical lines. Attractive behavior *near the solvent's critical point* is a necessary condition for supercritical solubility enhancement; repulsive behavior near the less volatile component's critical point is closely related to gas–gas immiscibility.

Introduction

The partial molar properties (volume, enthalpy, excess entropy with respect to an infinitely dilute ideal gas mixture at the same density and temperature) of an infinitely dilute solute diverge at the solvent's critical point. The solute acts as a local density perturbation whose effect is propagated over a length scale given by the correlation length. Its partial molar properties scale as the solvent's compressibility, and their divergence is a critical phenomenon, indicative of long-ranged correlations in density fluctuations. Although this divergence is common to every infinitely dilute near-critical system, its sign is not. For a given system, the solute's partial molar volume, enthalpy, and excess entropy diverge with the same sign, and can therefore tend either to $+\infty$ or to $-\infty$.

Short-ranged interactions occurring over distances of a few angstroms determine the sign of the diverging solute partial molar properties. In this paper we investigate the effects of differences in size, shape, and interaction energies between solute and solvent molecules upon the sign of the solute's diverging partial molar properties.

Understanding the relationship between solute–solvent differences in molecular size, architecture, and energetics, on the one hand, and bulk thermodynamic behavior, on the other, is especially important in the case of dilute mixtures of nonvolatile solutes in supercritical solvents. In this class of system, negative solute partial molar volumes and enthalpies near the mixture's lower critical end point give rise to a solubility increase with pressure (at constant temperature) and to a decrease in solubility with temperature (at constant pressure), respectively. For a nonvolatile solute, the mixture's lower critical end point is very close to the solvent's critical point. Since, furthermore, the mixture is dilute, the large and negative solute partial molar volume and enthalpy are a consequence of proximity to the solvent's critical point. Thus, the question naturally arises as to which aspects of molecular asymmetry between solute and solvent will give rise to negatively diverging partial molar properties.

Our theoretical study reflects the current widespread interest in the topic of molecular interactions in dilute, supercritical systems.[1,2] In recent years, experimental studies have probed the behavior of dilute supercritical mixtures over a range of length scales. Long-ranged correlations and cooperative behavior have been investigated via solute partial molar property measure-

(1) Brennecke, J. F.; Eckert, C. A. *AIChE J.* **1989**, *35*, 1409.
(2) Johnston, K. P.; Peck, D. G.; Kim, S. *Ind. Eng. Chem. Res.* **1989**, *28*, 1115.

0022-3654/91/2095-0386$02.50/0